Strain effects on the magnetic order of epitaxial FeRh thin films

H. Kumar, D. R. Cornejo, S. L. Morelhao, S. Kycia, I. M. Montellano, N. R. Álvarez, G. Alejandro, and A. Butera

Citation: Journal of Applied Physics **124**, 085306 (2018); doi: 10.1063/1.5020160
View online: https://doi.org/10.1063/1.5020160
View Table of Contents: http://aip.scitation.org/toc/jap/124/8
Published by the American Institute of Physics

Strain effects on the magnetic order of epitaxial FeRh thin films

H. Kumar,[1,a)] D. R. Cornejo,[1] S. L. Morelhao,[2,3] S. Kycia,[3] I. M. Montellano,[4,b)] N. R. Álvarez,[5] G. Alejandro,[6] and A. Butera[4,6,c)]

[1]*Laboratório de Materiais Magnéticos, Departamento de Física dos Materiais e Mecânica, Universidade de São Paulo, São Paulo, Brazil*
[2]*Instituto de Física Aplicada, Universidade de São Paulo, São Paulo, Brazil*
[3]*Department of Physics, University of Guelph, Guelph, Ontario N1G 1W2, Canada*
[4]*Instituto Balseiro (U. N. Cuyo), 8400 Bariloche, Río Negro, Argentina*
[5]*Centro Atómico Bariloche (CNEA) and Conicet, 8400 Bariloche, Río Negro, Argentina*
[6]*Instituto de Nanociencia y Nanotecnología (CNEA-Conicet), Centro Atómico Bariloche, 8400 Bariloche, Río Negro, Argentina*

(Received 20 December 2017; accepted 26 July 2018; published online 27 August 2018)

In this work, we report the experimental results obtained on a set of ∼90 nm thick FeRh epitaxial films deposited on MgO (001), MgO (111), and Al_2O_3 (0001) single crystal substrates. The magnetic characterization was achieved by measuring magnetization curves and ferromagnetic resonance as a function of temperature and orientation of the films with respect to the applied magnetic field. We discuss our results by comparing the characteristics of the antiferromagnetic-ferromagnetic transition among FeRh films of the same thickness but exposed to different post-growth annealings and deposited on substrates of different crystalline orientations. We have found that there is a correlation between the strain present in the films and their magnetic behavior, observing that a change in the in-plane stress from compressive to tensile tends to shift the magnetic transition by more than 60 K. The interplay between magnetic and elastic properties was further analyzed by ferromagnetic resonance, and we have found that the magnetoelastic component of the anisotropy varies from out-of-plane to in-plane, depending on the substrate. These findings could be of great importance if a precise tuning of the magnetic transition temperature or the magnetic anisotropy is needed for a specific application. *Published by AIP Publishing.*
https://doi.org/10.1063/1.5020160

I. INTRODUCTION

It is well known that bulk FeRh undergoes a very unusual transition from an antiferromagnetic (AF) α'' to a ferromagnetic (FM) α' phase upon heating from room temperature (RT) to above $T_{AF-FM} \approx 300 - 370$ K, preserving the crystal symmetry and accompanied by ∼1% lattice expansion.[1–4] In the α'' phase, Fe spins are ordered AF in the [001] direction, with a net magnetic moment of 3.3 μ_B, while Rh ions display no magnetic moment. In the α' phase, all the spins are aligned ferromagnetically, also in the [001] direction, with a magnetic moment of 3.2 μ_B contributing from the Fe and 0.9 μ_B from the Rh atoms.

The crystal structure of the $Fe_{50}Rh_{50}$ alloy is CsCl type, and the AF-FM transition is of first order with a thermal hysteresis of the order of 10 K in bulk materials. In Fig. 1, we reproduce schematically the bulk phase diagram reported in Ref. 3, focused on the magnetic behavior around the 50% composition region. Note that the AF-FM transition temperature tends to increase by more than 50 K when the Rh concentration changes from 50% to 55%. Fe-rich alloys display a bcc α phase that converts into the paramagnetic (PM) fcc γ phase at high temperatures. The $\alpha \leftrightarrow \gamma$ transition is of martensitic type.[5] According to Ref. 2, the γ phase can be retained at room temperature by rapid quenching from the γ field for alloys between 25% and 40% Rh. In thin films, the phase diagram and their boundaries are not clearly established yet, so the presence of small amounts of secondary phases, like the bcc α (FM) or fcc γ (PM), is often observed in nearly equiatomic FeRh films.[6,7]

Although FeRh is not the only compound that develops this unusual AF to FM transition,[8] it is indeed unique in the sense that T_{AF-FM} can be significantly above room temperature. Beyond the basic interest in the underlying physics, this feature makes FeRh a very interesting material for technological applications, such as thermally assisted magnetic recording[9] or resistive memories.[10] Although the bulk binary system (Fe, Rh) has been extensively studied since the 1940s and rather complete phase diagrams were obtained, work in FeRh thin films has only started relatively recently because of the potential applications in magnetic storage.[6,7,9,11–15] There is experimental evidence that substitutional doping,[16] magnetic field,[11] strain,[17] film thickness,[13] etc., can be used to modify and tune the magnetic behavior. Until 2014, most studies were focused on (001)-oriented FeRh films deposited on MgO(001), and it is only very recently that piezoelectric $BaTiO_3$ (BTO) and ferroelectric $0.72PbMg_{1/3}Nb_{2/3}O_3$–$0.28PbTiO_3$ substrates are being used.[18] Recently, Cherifi *et al.*[19] reported the electric field controlled phase transition in the FeRh/$BaTiO_3$ heterostructure: electric field controlled piezoelectric strains in the BTO substrate allow to change the T_{AF-FM} transition by 25 K.

[a)]Present address: Department of Sciences and Humanities, NIT Uttarakhand, Srinagar 246174, India.
[b)]Present address: Max Planck Institut fur Plasmaphysik, Garching bei Munchen, Germany.
[c)]Electronic mail: butera@cab.cnea.gov.ar

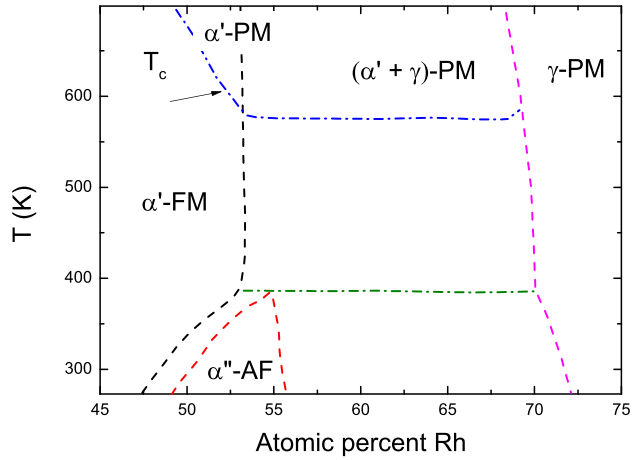

FIG. 1. Phase diagram of the binary (Fe, Rh) bulk alloy around the equiatomic composition. Adapted from Ref. 3.

Therefore, recent studies demonstrate that electric field controlled substrate strain is a key parameter to control the FeRh phase transition. Additionally, new efforts have been concentrated in understanding the effects of film strain on the magnetic and transport properties of FeRh films.[20,21] In this context, and to complement these studies, we report in this article the interplay between magnetism and substrate induced strain effects on FeRh thin films deposited on different single crystal wafers. In particular, we have studied the growth of FeRh thin films deposited on MgO (001), MgO (111), and Al_2O_3 (0001) substrates. In our work, at difference of other reports, the chosen substrates induce different epitaxial orientations of the films.

II. EXPERIMENTAL PROCEDURE

FeRh thin films with nominally equiatomic composition were deposited at 5 mTorr Ar pressure onto MgO (001), MgO (111), and Al_2O_3 (0001) (c–Al_2O_3) single crystal substrates by dc magnetron sputtering from separate Fe and Rh targets (99.99% purity) in an AJA 2000 sputtering system. The films were all grown at the same time and were not capped. The deposition process to obtain films with good epitaxial grow was optimized at $T = 525\,^{\circ}\mathrm{C}$, a rate of $\sim$0.03 nm/s, and a base pressure of 1.2×10^{-6} Torr. The nominal thickness of the films was chosen to be approximately 90 nm and was afterwards determined by Rutherford Backscattering Spectrometry (RBS). We did not detect oxygen in the RBS composition analysis of the samples. The crystal structure of the FeRh thin films was probed with x-ray diffraction (XRD) experiments that were conducted in a Rigaku Ultima theta-theta system and a 3-circle Huber diffractometer ($\lambda = 0.154056$ nm) at IF-USP (Brazil). Complementary phi-scans were performed using a 4-circle Huber diffractometer ($\lambda = 0.154056$ nm) of the X-ray Laboratory of the University of Guelph (Canada).

The magnetic characterization of the samples was accomplished by performing dc magnetization (M) and ferromagnetic resonance (FMR) experiments. The magnetization measurements were conducted in a home-made Faraday balance magnetometer, operating between 280 K and 1000 K, with a maximum applied field (H) of 1 T. In this experimental setup, the direction of the magnetic field is always parallel to the film plane. FMR spectra were acquired using a commercial Bruker ESP300 spectrometer operating at a microwave frequency of 9.4 GHz (X band). The samples were placed in the center of a rectangular resonant cavity, where the derivative of the absorbed power was measured using standard field modulation and lock-in detection techniques with amplitudes in the range of 5–20 Oe. The samples could be rotated inside the resonator in order to collect the spectra for different orientations of the films, and the temperature dependent experiments were performed in the range of 300–480 K.

III. EXPERIMENTAL RESULTS

A. Film growth and epitaxy

The composition and thickness of each sample were determined by using RBS. For the films used in this study, we have determined a 55% at. Rh and a thickness of 92 nm. The rest of the relevant parameters are summarized in Table I. Most of the samples were post-annealed at $T \sim 700\,^{\circ}\mathrm{C}$ for four hours in vacuum to promote the atomic order of Fe and Rh species. The quality of the films was tested by x-ray diffraction measurements at room temperature. We have found that in all cases the diffraction patterns show a majority α-bcc phase with traces of the γ-fcc structure in some films, which could not be completely removed even after annealing. XRD results also indicate (see Fig. 2) that all films grew with a strong texture that depends on the type of substrate. It is clear from the figure that annealed films deposited on MgO (001), MgO (111), and c–Al_2O_3 substrates develop strong [001], [011], and [111] textures, respectively. As an exception, the as-grown film on c–Al_2O_3 (not shown) grows with a predominant [011] texture which turns to a [111] (superstructure) preferred orientation after annealing, indicating a higher degree of atomic order. The room temperature out-of-plane (OOP) lattice parameter c was estimated from the diffraction peak positions of the (002), (022), and (111) Bragg reflections of FeRh films deposited on MgO (001), MgO (111), and c–Al_2O_3 substrates. We obtained $c = 0.3021(3)$ nm, $c = 0.2993(3)$ nm, and $c = 0.2980(3)$ nm, respectively. As a reference, the room temperature cubic lattice parameter of $Fe_{45}Rh_{55}$ reported in polycrystalline films deposited on Si substrates (α'' phase) is $a_0 = 0.2994(7)$ nm.[15]

In the case of the sample 7M100, the FeRh lattice is rotated by 45° around the growth direction with respect to

TABLE I. Name of the different samples used in this study with their relevant parameters. In all cases, the Rh concentration is 55% atomic and the film thickness is 92 nm. We indicate in bold characters the dominant crystalline texture.

Sample	Substrate	Post-annealing	Orientation of the film	ε_z
7M100	MgO (001)	700 °C	**[001] bcc**	6.9×10^{-3}
7M111	MgO (111)	700 °C	**[011] bcc** + [111] fcc	-2.4×10^{-3}
7A01	Al_2O_3 (0001)	700 °C	**[111] bcc** + [002] fcc	-6.9×10^{-3}
A01	Al_2O_3 (0001)	No	**[011] bcc** + [111] bcc	…

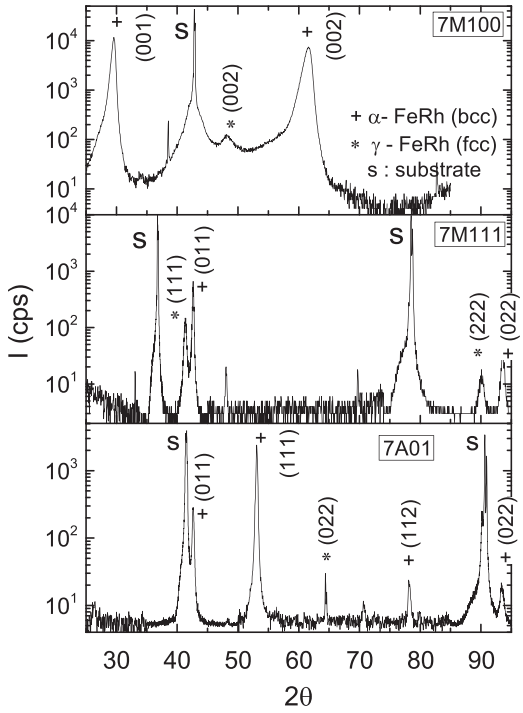

FIG. 2. X-ray diffraction patterns of $Fe_{45}Rh_{55}$ films deposited on MgO(001), MgO(111), and Al_2O_3(0001) substrates. Diffraction peaks from the film and from the substrate are indicated on the patterns.

the MgO (001) substrate. In other words, the in-plane [110] direction of the film is aligned to the in-plane [100] direction of the substrate lattice. In this situation, the film lateral lattice parameter ($a_0\sqrt{2} = 0.4243$ nm) has to be strained by 0.7% to perfectly match the substrate ($a_{MgO} = 0.4212$ nm). When the film is strained, the lattice mismatch produces a tetragonal distortion in the FeRh unit cell, expanding along the out-of-plane [001] direction and compressing along both [100] and [010] in-plane directions. Using the out-of-plane lattice parameter $c = 0.3021(3)$ nm from x-ray diffraction, the reported[22] Poisson's ratio ($\nu \sim 0.32$), $a_s = a_{MgO}/\sqrt{2}$, and the strain equations for a fully strained film (where a_s is the substrate lattice parameter)

$$c = a_0(1+\varepsilon_z), \quad \varepsilon_z = \left(\frac{2\nu}{\nu-1}\right)\varepsilon_x, \quad \varepsilon_x = \frac{a_s - a_0}{a_0}, \qquad (1)$$

we estimated the cubic lattice parameter $a_0 = 0.3000(3)$ nm, very close to the bulk lattice parameter of $Fe_{45}Rh_{55}$.

We note that this assumption is strictly valid below a critical thickness d_{cr}, that is the threshold above which the stress-induced distortions begin to gradually relax.[19] For instance, a previous report[11] shows that strain effects are observable in 110 nm films deposited on MgO (001) and Al_2O_3 (0001) although 110 nm is larger than the estimated critical thickness ($d_{cr} \sim 50$ nm).

In a simple model, d_{cr} depends only on the lattice mismatch between the film and the substrate through the relation[21] $d_{cr} = a_0 a_s/2(a_0 - a_s)$. Using this definition, we obtained $d_{cr} \sim 20$ nm for the 7M100 sample, which is in the range reported by other authors (12 nm–50 nm).[21,23] Therefore, as d_{cr} is smaller than our film thickness (90 nm), the above definition ε_x is an upper limit for the in-plane strain.

Note that although the films have been fabricated above the AF-FM transition and that FeRh undergoes a relatively large decrease in volume at the magnetic transition when cooling down (as reported in Refs. 4 and 24), the FeRh lattice still matches that of the MgO substrate at RT. We have performed temperature-dependent measurements of the in-plane and out-of-plane lattice parameters on an FeRh sample grown on MgO (001) with a slightly different composition (not shown). We found that in the FM region, at T = 453 °C, the tetragonal distortion is also present with a strain $\varepsilon_z \sim 0.01$.

The quality of the out-plane data suggests that the films are epitaxially oriented. This was confirmed by performing an asymmetric phi-scan on the $Fe_{45}Rh_{55}$ film and comparing it to that corresponding to the substrate. The in-plane epitaxial relation of the $Fe_{45}Rh_{55}$(001) film on MgO(001) was explored by first aligning to the symmetric MgO(001) and asymmetric MgO(420), and then aligning to symmetric $Fe_{45}Rh_{55}$(001) and asymmetric $Fe_{45}Rh_{55}$(210) at room temperature.

The phi-scan diffractograms of samples 7M100, 7M111, and 7A01 are shown in Fig. 3. In the case of 7M100, both the MgO(001) substrate and the $Fe_{45}Rh_{55}$(001) oriented film have four-fold symmetry. As can be seen in Fig. 3(a), the matching between substrate and film is better fulfilled if the [100] direction of the film is rotated by 45° with respect to the [100] direction of the substrate.

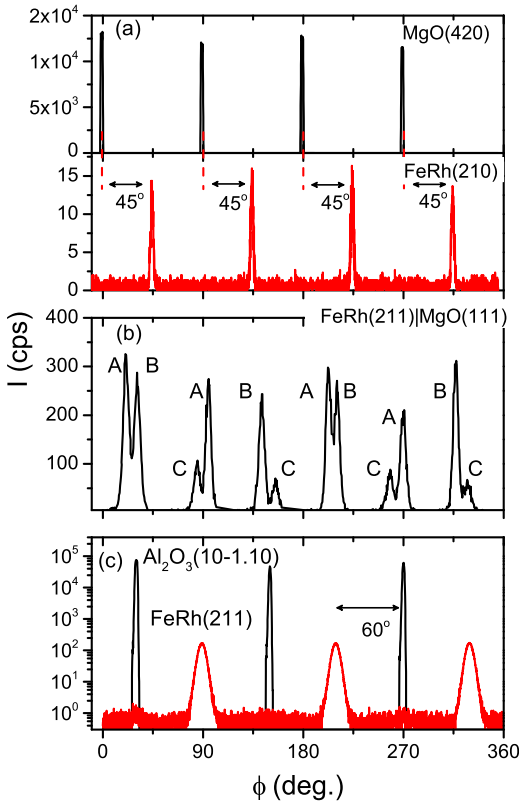

FIG. 3. Phi-scan diffractograms of (a) 7M100, (b) 7M111, and (c) 7A01 samples. In (a), the radial angle was set to $\chi = 26.6°$ showing the 45° rotation of the FeRh cubic cell with respect to the MgO(001) substrate. In (b), $\chi = 30°$ and the three different domains (A, B, C) of (011) bcc on (111) planes can be distinguished. In (c), we show the asymmetric (10–1.10) and (211) reflections for the Al_2O_3 substrate and the film, respectively.

In the case of MgO(111) substrates, the films tend to grow with a [011] texture of the bcc phase, and a minor [111] textured fcc-phase, which could not be removed even after annealing at 700 °C. We have found that even though the lattice mismatch between both lattices is relatively large, the interplanar (011) distance perpendicular to the film plane [$d_{011} = 0.2117(2)$ nm] is slightly smaller than that expected for a relaxed FeRh lattice ($d0_{011} = 0.2121$ nm), giving a strain $\varepsilon_z = -2.4 \times 10^{-3}$.

As can be seen in Fig. 3(b), the phi-scans of the (211) FeRh reflections show six double peaks consistent with the three possible domains (A, B, C) of bcc (011) planes on an fcc (111) surface, which repeat each 60°, and an angular separation between ⟨211⟩ axes of 70.5°. Two different epitaxies are often found when bcc compounds are deposited on fcc (111) surfaces. In both situations, the matching plane is the bcc(011),[25] but in one case the in-plane orientation relationship is [110]bcc//[112]fcc (Nishiyama-Wasserman), and in the other [111]bcc//[110]fcc (Kurdjumov-Sachs). The phi-scans are consistent with only one epitaxy, although a conclusive identification was not possible.

As we have already mentioned, [110] and [111] textures were observed in as-deposited and annealed films on c–Al_2O_3. In this aspect, Yuasa *et al.*[26] reported that the epitaxial nature of $(Fe, Rh)_{95}Ir_5$ films deposited on $Al_2O_3(0001)$ substrates depends upon the sputtering rate, in such a way that in the range 0.02 nm/s–0.06 nm/s, both (011) or (111) oriented films can be obtained. In our case, annealed FeRh films deposited on c–Al_2O_3 substrates develop a strong [111] out of plane texture. The epitaxial growth was further analyzed using phi-scans [see Fig. 3(c)]. We have found an in-plane epitaxy with the relationship $Fe_{45}Rh_{55}$ (Refs. 1–10)// Al_2O_3.[11–20] As the in-plane cell size of the substrate is larger than that corresponding to the film by approximately 10%, an in-plane tensile strain is expected for FeRh on c–Al_2O_3. This, in turn, produces a compressive strain in the out-of-plane direction. From the diffractograms we have deduced the interplanar distances $d_{111} = 0.1720(2)$ nm and $d0_{111} = 0.1732(2)$ which can be used to estimate the out-of-plane and in-plane strains, $\varepsilon_z = -6.9 \times 10^{-3}$ and $\varepsilon_x = 7.2 \times 10^{-3}$.

In Table II, we summarize the results of this subsection for samples 7M100, 7M111, and 7A01. The out-of-plane parameter c was determined directly from the XRD diffractograms at RT. Additionally, the in-plane parameters a, ε_x, and ε_z were all calculated using the relaxed cubic value $a_0 = 0.3000(2)$ nm (common for all the samples). Note that in-plane parameters were estimated under the hypothesis of uniform biaxial stress using the reported Poisson ratio, $\nu = 0.32$.

TABLE II. Measured and calculated out-of-plane and in-plane cell parameters and strain values at room temperature.

Sample	c (nm)	a (nm)	c/a	ε_z	ε_x
7M100	0.3021(3)	0.2978	1.0145	0.0069	−0.0073
7M111	0.2993 (3)	0.3007	0.9952	−0.0024	0.0025
7A01	0.2980 (3)	0.3021	0.9863	−0.0069	0.0072

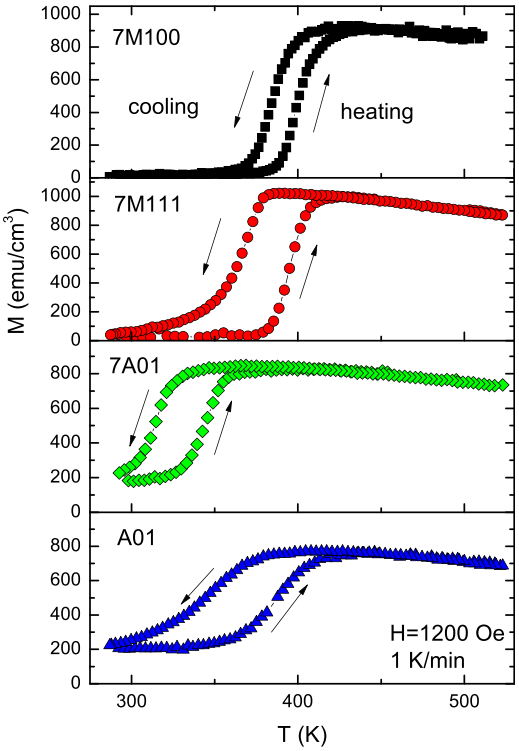

FIG. 4. Magnetization vs. temperature cycles performed on samples 7M100, 7M111, 7A01, and A01. The static magnetic field $H = 1200$ Oe was applied parallel to film plane at a heating/cooling rate of 1 K/min.

Although the composition of our films is different from that reported in Ref. 11, a similar trend for the strain of FeRh on MgO(001) and c–Al_2O_3 was found. Note that by using different substrates the in-plane strain can be changed from compressive [MgO (001)] to tensile (c–Al_2O_3), which is expected to reflect in the magnetic properties of the films. For example, the tensile stress of FeRh films on the sapphire substrate could be expected to decrease the AF-FM transition temperatures because the larger cell size induces the stabilization of the ferromagnetic phase at lower temperatures.[17]

B. Magnetization

In Fig. 4, we plot typical magnetization vs. temperature cycles, obtained from samples 7M100 (top), 7M111 (center), and 7A01-A01 (bottom) while cooling and heating them inside a Faraday balance magnetometer with an applied field $H = 1200$ Oe parallel to the film plane.

At room temperature, the magnetization is very close to zero for samples 7M100 and 7M111 (annealed), which is consistent with the α''-AF state. Upon heating, the magnetization gradually increases according to the growing fraction of the α'-FM phase. The maximum magnetization value for these films reaches $M_s^{max} \sim 1025$ emu/cm^3 at $T = 392$ K in the cooling branch of the 7M111 film. This value of M_s is within the broad range of reported data[7,11–13,27,28] for different FeRh films with $M_s^{max} \approx 700 - 1200$ emu/cm^3. For temperatures above 420 K, the AF-FM transition seems to be complete for all samples, but a strong dependence with the substrate was found. Upon cooling, we observe a hysteretic

behavior, which confirms the first order character of the phase transition.

We have defined the transition temperatures T^h_{AF-FM} (heating) and T^c_{AF-FM} (cooling) as the points where the magnetization reaches 90% of its maximum and the corresponding difference $\Delta T = T^h_{AF-FM} - T^c_{AF-FM}$. This criterion was adopted to facilitate the comparison with the FMR data presented in Sec. III C. In Table II, we summarize the results for the 55% Rh samples: 7M100, 7M111, 7A01, and A01. In the case of annealed films, the AF-FM transition of the heating branch decreases from $T^h_{AF-FM} = 418$ K for 7M100 to $T^h_{AF-FM} = 355$ K for 7A01. As already mentioned when the crystallographic results were discussed, this behavior is consistent with the systematic change that occurs in the in-plane strain, from compressive to tensile, when MgO (001), MgO(111), and c–Al_2O_3 are used as substrates. The transition temperature $T^h_{AF-FM} = 418$ K for 7M100 is considerably larger than the values reported in Refs. 11–13 and 28, which average $T^h_{AF-FM} = 400$ K. However, all those films correspond to the composition $Fe_{49}Rh_{51}$, while our samples have 55% Rh, which was already shown[2] in Fig. 1 to shift the transition to higher temperatures. Apart from composition, differences may also arise in the strong dependence of the transition temperature on the applied magnetic field, film thickness,[29] and the magnetic and thermal history.[11] For the sample 7A01, we obtained $T^h_{AF-FM} = 355$ K which is very close to the value reported in Ref. 11 ($T^h_{AF-FM} \sim 360$ K). The non-zero magnetization observed at RT for this sample is due to the incomplete FM-AF transition at the lowest temperature we could reach with our magnetometer.

The width of the temperature hysteresis (ΔT) is larger in 7M111 and 7A01 ($\Delta T \sim 30$ K) than in 7M100 ($\Delta T \sim 20$ K). This could be induced by the presence of a relatively larger fraction of the γ-paramagnetic phase, as shown in Ref. 13. In the case of the non-annealed A01 sample, this broadening effect is enhanced by the partial disorder of Fe and Rh atoms in the bcc phase and the presence of the fcc γ-phase.

C. Ferromagnetic resonance (FMR)

To follow the evolution of the magnetic phases and determine the presence of anisotropies, we recorded FMR spectra at different temperatures, both heating and cooling from RT up to ~480 K in each sample. In these experiments, the static magnetic field was applied perpendicular to the film plane, as we found that the conditions for the detection of the resonant absorption of the incident microwaves were optimal for this orientation.

A standard FMR spectrum is the first derivative of the microwave power absorption of the sample with respect to the "static" magnetic field, H, which is slowly swept across a predefined field range. The field value at which the derivative is zero is defined as the resonance field (H_{res}), and the distance between a derivative maximum and minimum is called the peak-to-peak linewidth (ΔH_{pp}) .

In Fig. 5, we plot a series of typical spectra recorded while decreasing the temperature from 455 K to 360 K for the sample 7M111. The qualitative features of the rest of the annealed samples are quite similar although the characteristic

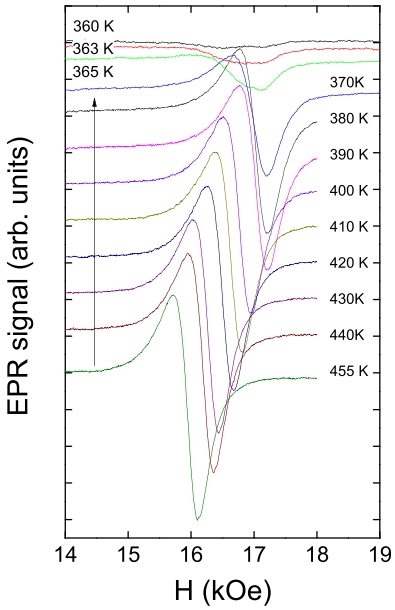

FIG. 5. FMR spectra of the annealed 7M111 sample recorded while cooling. The static magnetic field H was set normal to the film plane. Spectra have been vertically shift for clarity. A similar behavior was observed for the other films.

temperatures are different. From $T \approx 380$ K and above, the FMR line is well defined and we can safely assume that the sample is completely in the α'-FM phase. We observe that when the temperature is decreased, the resonance field moves to higher values. At the same time, the linewidth increases and the intensity progressively diminishes until it virtually vanishes, and we can suppose that the sample is completely in the α''-AF phase. From the spectra measured for the different films, we extracted the temperature behavior of the resonance field and the linewidth. In Fig. 6, we present these variables as

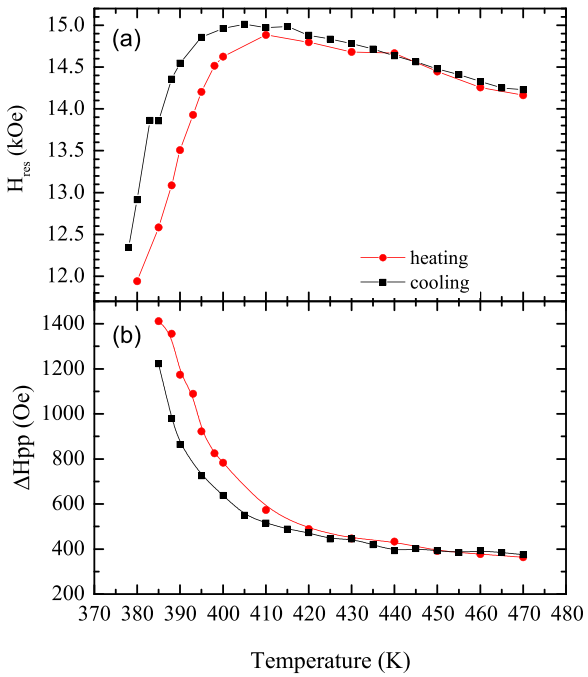

FIG. 6. H_{res} (a) and linewidth ΔH_{pp} (b) as a function of temperature for the annealed 7M100 sample. The experiments were done subsequently heating (circles) and cooling (squares).

TABLE III. Transition temperature T_{AF-FM} (heating and cooling the films) and width of the thermal hysteresis estimated from dc magnetization and FMR experiments (all in K). The error in the determination of the temperature is indicated in parentheses.

Sample	T_{AF-FM} (K) (heating) DC/FMR	T_{AF-FM}(K) (cooling) DC/FMR	ΔT(K) DC/FMR
7M100	418/410	398/400	20/10(5)
7M111	406/398	376/375	30/23(5)
7A01	355/360	327/325	28/25(5)
A01	408/425	368/400	40/25(5)

a function of T for the 7M100 sample. The temperature behavior of the FMR resonance parameters obtained for the 7M100 film is representative of the other annealed samples, so the following discussion applies for all of them.

The FMR cycles also present temperature hysteresis (ΔT) whose value depends on the substrate, as we can see from Table III. We can distinguish two different temperature regimes, which is more evident in H_{res} vs. T in Fig. 6(a): a "high-T" regime where H_{res} increases when the temperature is decreased until it reaches a maximum, and a "low-T" regime where H_{res} diminishes rapidly with decreasing temperature. From the H_{res} vs. T curves, we obtained the temperature of the magnetic transition (T_{AF-FM}), by determining the point at which H_{res} vs. T is maximum. When we cool the sample from the high temperature α'-FM region down to RT, we approach gradually the temperature and field where the sample becomes entirely AF. Thus, the maximum of the H_{res} vs. T curve signals the temperature where the AF phase progressively begins to nucleate and the AF and FM phases start to coexist. In Table III, we summarize the values of T_{AF-FM} (heating and cooling) and the width of the thermal hysteresis (ΔT) for the measured samples and compare these values with those obtained from dc magnetization experiments. A very good agreement is observed in the case of annealed films, even though the criterion for the determination of T_{AF-FM} is not necessary equivalent in the two experimental techniques. These results also show that T_{AF-FM} is clearly substrate-dependent and reveal the influence of stress/strain effects due to the lattice mismatch between the substrate and the film. The highest and lowest T_{AF-FM} were measured on the 7M100 and 7A01 films, respectively, which is fully consistent with the magnetization results.

Ferromagnetic resonance can also be used to obtain information about the magnetic anisotropies of the system. The anisotropy terms generally found in ferromagnetic films are in most cases of magnetocrystalline, magnetoelastic, or shape (dipolar) origin. The magnetocrystalline anisotropy (MCA) is an intrinsic property of the material closely related to the spin orbit coupling and usually reflects the symmetry of the crystal structure. The origin of the magnetoelastic anisotropy is usually extrinsic and related to residual stresses introduced in the films during the growth process that induce a preferential axis (or plane) of easy magnetization. The shape anisotropy is a direct consequence of the dipolar interaction which produces a demagnetizing field, and in the case of a thin film it provides an easy-plane of magnetization parallel to the film.

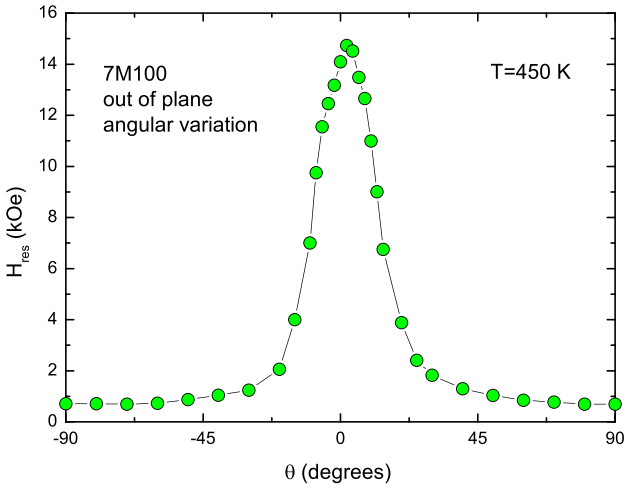

FIG. 7. Angular variation of the resonance field, H_{res}, in the OOP configuration for the sample 7M100 at $T = 450$ K. θ is the angle between the magnetic field, H, and the film plane.

In order to study the magnetic anisotropies of our samples, we performed FMR experiments varying the orientation of the external field, H, with respect to the film and collecting the resonance spectra at different angles. We performed the experiments using the out-of-plane (OOP) experimental setup where H is rotated from the film plane to the normal of the film. In some cases, we also acquired spectra rotating the magnetic field parallel to the film plane. From these FMR measurements, it is possible to obtain information about the anisotropies present in the samples.

Experiments were recorded for all samples for $T > T_{AF-FM}$, choosing the temperature to ensure that the film was completely in the ferromagnetic phase. In Fig. 7, we show an OOP angular variation of the resonance field H_{res} for the sample 7M100. A similar behavior was observed in the other films. The OOP angular variation of H_{res} in Fig. 7 is typical of a thin film for which the easy plane of magnetization coincides with the film itself, as expected.

To quantify our results, we used the Smit-Beljers model for a thin film[30] with shape plus uniaxial anisotropy with the same symmetry, which leads to the Kittel expressions with an effective field H_{eff} that can be estimated from the resonance field parallel ($H_{//}$) and perpendicular ($H_{\perp}$) to the film plane[31,32]

$$\frac{\omega}{\gamma} = \sqrt{H_{//}\left(H_{//} + H_{eff}\right)}, \tag{2}$$

$$\frac{\omega}{\gamma} = H_{\perp} - H_{eff}, \tag{3}$$

TABLE IV. Saturation magnetization, perpendicular resonance field, effective anisotropy, perpendicular anisotropy, and magnetoelastic anisotropy for FeRh films deposited on different substrates.

Sample	M_s (emu/cm^3)	$H_{\perp}$ (Oe)	H_{eff} (Oe)	$H_A^{\perp}$ (Oe)	H_A^{ME} (Oe)
7M100	925	14 447	11 087	+537	+720
7M111	1004	16 450	13 090	−473	−226
7A01	830	15 600	12 240	−1810	−793
A01	760	13 580	10 220	−670	…

where $H_{\text{eff}} = 4\pi M_s - H_A^{\perp}$. $4\pi M_s$ is the shape anisotropy of a thin film and $H_A^{\perp}$ accounts for additional contributions to the magnetic anisotropy normal to the film plane. $\omega = 2\pi f$ is the driving angular frequency and $\gamma = g\mu_B/\hbar$ is the gyromagnetic factor, with $g \sim 2.09$ for Fe and ferromagnetic iron alloys,[32–34] μ_B is the Bohr magneton, and $\hbar$ is the reduced Planck constant. Because the magnetization for the parallel mode was not fully saturated in X band experiments, we only used the second Kittel equation and the values of M_s reported in Sec. III B to estimate $H_A^{\perp}$ for the different samples. In some of the films, we have found a small in-plane anisotropy which was not necessary to consider in the present analysis. Results are presented in Table IV.

From the data shown in Table IV, it is readily observed that the perpendicular anisotropy $H_{\text{A}}^{\perp}$ is maximum for the film 7M100, decreases and changes sign for 7M111, and reaches a minimum for 7A01. Note that a positive $H_{\text{A}}^{\perp}$ represents an anisotropy favoring the alignment of M perpendicular to the film plane, while a negative $H_{\text{A}}^{\perp}$ tends to align M inside the film. According to the crystallographic results, the sample 7M100 has an in-plane strain, 7M111 shows a relatively small tensile stress, and 7A01 has a much larger tensile stress. In a simple model, the magnetoelastic anisotropy coefficient may be written as $K_{ME} = -\frac{3}{2}\lambda\sigma_x = \frac{3}{2}\lambda\frac{\varepsilon_x Y}{2\nu}$, where Y is the Young's modulus and λ the linear saturation magnetostriction. Reported values[22,35] of bulk FeRh are $Y \sim 1.9 - 2.1 \times 10^{12}$ dyn/cm^2. For the magnetostriction in the FM phase, there is a range of values[4,35,36] from $\lambda \sim 0.5 - 1 \times 10^{-5}$ to $\lambda \sim 10^{-4}$, which depends on the temperature region and the maximum field used for the estimation of λ. If the additional anisotropy term is assumed to be of magnetoelastic origin, it may be related to an anisotropy field by $H_A^{\text{ME}} = 2K_{ME}/M_s$. Using an average value for $\lambda \sim 1 \times 10^{-5}$ and the strain calculated from the XRD data, we obtained the values shown in the last column of Table IV. We observed a reasonably good agreement between $H_{\text{A}}^{\perp}$ and H_A^{ME} which indicates that most of the observed effects are of magnetoelastic origin. The systematic larger values of H_A^{ME} may be due to an underestimation of the relaxed lattice parameter a_0.

It is interesting to compare our results in Tables II–IV with recent experimental results that present the dependence of T_{AF-FM} on c/a ratio[20,21] and with *ab initio* calculations[27,37] of the magnetocrystalline anisotropy (MCA) vs. c/a. We observed that both DC and FMR of measurements show an increasing behavior of T_{AF-FM} with c/a, consistent with the results reported in Ref. 20 for 100 nm films deposited on different substrates. Also, by comparing the points in the FM field of the phase diagram of Ref. 27 with our data, we observe that there is a nice agreement if we make a correspondence between MCA and our magnetoelastic term, H_A^{ME}. Indeed, we obtained a negative (out of plane) anisotropy that tends to lift the magnetization vector from the film plane for sample 7M100 ($c/a > 1$) and a positive (in-plane) anisotropy that tends to keep M vector in the film plane for samples 7M111 and 7A01 ($c/a < 1$).

As we already mentioned, we have found a relatively small in-plane uniaxial anisotropy in some of the films (for example, 7M100) in which a variation of H_{res} with cubic symmetry was expected. This observation is also consistent with the influence of magnetoelastic effects on the magnetic behavior of the films.

IV. CONCLUSIONS

We have grown highly oriented FeRh thin films onto MgO and Al_2O_3 substrates of different crystalline orientations by conventional sputtering techniques. Most of the samples were annealed at 700 °C in order to induce the chemical order of the Rh and Fe atoms, the reduction of the residual γ phase, and the promotion of the AF-FM transition. The properties of this unusual transition, which occurs between 325 K and 420 K depending on the sample and the magnetothermal history, were studied by magnetization and FMR experiments. We observed a thermal hysteresis consistent with a first order transition in the FMR measurements. We determined the transition temperature $T_{\text{AF–FM}}$ and found that it depends on the kind of substrate and growth orientation. This was ascribed to the differences in the stresses experienced by the films due to the specific mismatch between film and substrate lattice parameters. From the temperature dependence of the resonance field and the linewidth, we have determined a phase coexistence region AF-FM, as suggested by the reduction of H_{res} when the temperature is decreased. This fact coincides with the abrupt increase in the peak-to-peak linewidth, which is also consistent with this picture. The resonance field perpendicular to the film plane was used to estimate the perpendicular anisotropy in the different samples. Concerning the magnetic anisotropies of our FeRh films, the angular variation of the resonance field measured in the out-of-plane configuration is the one expected for a thin film dominated by the shape anisotropy, which tends to place the magnetization vector in the film plane, plus other extra contributions also perpendicular to this plane. The interpretation of our structural and FMR results led us to conclude that the main contribution to the magnetic anisotropy originates mainly in magnetoelastic effects.

Finally, the analysis of the angular dependence of H_{res} measured using the in-plane configuration supports the hypothesis that there is a prevailing in-plane uniaxial anisotropy, arising also from stress effects, which dominates over the expected four-order symmetry expected from pure magnetocrystalline terms.

ACKNOWLEDGMENTS

This work was partially supported by Conicet under Grant No. PIP 201501-00213, ANPCyT Grant No. PICT 2013-0401, and U.N. Cuyo Grant No. 06/C484 (Argentina). H. Kumar acknowledges FAPESP (Brazil) for providing the postdoctoral fellowship (process 2010/18590-0) to develop this work and S. Morelhao acknowledges CAPES (Brazil) for process No. 88881.119076/2016-01. The technical support from Rubén E. Benavides, César Pérez, Matías Guillén (Argentina) and Sergio Romero, Antonio Carlos Franco da Silveira, Társis Mendes Germano, and Tiago Fiorini da Silva (IFUSP, Brazil) is deeply acknowledged.

[1]M. Fallot and R. Rocart, Rev. Sci. **77**, 498 (1939).
[2]G. Shirane, C. W. Chen, P. A. Flinn, and R. Nathans, Phys. Rev. **131**, 183 (1963).

[3]L. J. Swartzendruber, Bull. Alloy Phase Diagrams **5**(5), 456 (1984).
[4]M. R. Ibarra and P. A. Algarabel, Phys. Rev. B **50**, 4196 (1994).
[5]M. Fallot, Ann. Phys. **11**(10), 291 (1938).
[6]J. van Driel *et al.*, J. Appl. Phys. **85**, 1026 (1999).
[7]Y. Othani and I. Hatekayama, J. Appl. Phys. **74**, 3328 (1993).
[8]M. K. Chattopadhyay, S. B. Roy, A. K. Nigam, K. J. S. Sokhey, and P. Chaddah, Phys. Rev. B **68**, 174404 (2003); S. B. Roy, G. K. Perkins, M. K. Chattopadhyay, A. K. Nigam, K. J. S. Sokhey, P. Chaddah, A. D. Caplin, and L. F. Cohen, Phys. Rev. Lett. **92**, 147203 (2004).
[9]J.-U. Thiele, S. Maat, and E. E. Fullerton, Appl. Phys. Lett. **82**, 2859 (2003).
[10]X. Marti, I. Fina, C. Frontera, J. Liu, P. Wadley, Q. He, R. J. Paull, J. D. Clarkson, J. Kudrnovský, I. Turek, J. Kuneš, D. Yi, J.-H. Chu, C. T. Nelson, L. You, E. Arenholz, S. Salahuddin, J. Fontcuberta, T. Jungwirth, and R. Ramesh, Nat. Mater. **13**, 367–374 (2014).
[11]S. Maat, J.-U. Thiele, and E. E. Fullerton, Phys. Rev. B **72**, 214432 (2005).
[12]S. Inoue *et al.*, J. Appl. Phys. **103**, 07B312 (2008).
[13]I. Suzuki, J. Appl. Phys. **105**, 07E501 (2009).
[14]E. Mancini *et al.*, J. Phys. D.: Appl. Phys. **46**, 245302 (2013).
[15]H. Kumar, M. C. A. Fantini, and D. R. Cornejo, IEEE Trans. Mag. **49**, 4506 (2013).
[16]N. V. Baranov and E. A. Baranova, J. Alloys Compd. **219**, 139 (1995).
[17]C. W. Barton, T. A. Ostler, D. Huskisson, C. J. Kinane, S. J. Haigh, G. Hrkac, and T. Thomson, Sci. Rep. **7**, 44397 (2017).
[18]Y. Liu *et al.*, Nat. Commun. **7**, 11614 (2016); J. Chen *et al.*, J. Appl. Phys. **121**, 194101 (2017); Y. Lee *et al.*, Nat. Commun. **6**, 5959 (2015); Q. B. Hu *et al.*, Appl. Phys. Lett. **110**, 222408 (2017).
[19]R. O. Cherifi, V. Ivanovskaya, L. C. Phillips, A. Zobelli, I. C. Infante, E. Jacquet, V. Garcia, S. Fusil, P. R. Briddon, N. Guiblin, A. Mougin, A. A. Ünal, F. Kronast, S. Valencia, B. Dkhil, A. Barthélémy, and M. Bibes, Nat. Mater. **13**, 345 (2014).
[20]A. Ceballos, Z. Chen, O. Schneider, C. Bordel, L.-W. Wang, and F. Hellman, Appl. Phys. Lett. **111**, 172401 (2017).
[21]M. G. Loving, R. Barua, C. Le Graët, C. J. Kinane, D. Heiman, S. Langridge, C. H. Marrows, and L. H. Lewis, J. Phys.: D **51**, 024003 (2017).
[22]S. B. Palmer, P. Dentschuk, and D. Melville, Phys. Status Solidi (a) **32**, 503 (1975).
[23]C. Baldasseroni, "In-situ microscopy of the first-order magnetic phase transition in FeRh thin films," Ph.D. dissertation (University of California, Berkeley, 2013).
[24]D. W. Cooke, F. Hellman, C. Baldasseroni, C. Bordel, S. Moyerman, and E. E. Fullerton, Phys. Rev. Lett. **109**, 255901 (2012).
[25]K. Shikada, K. Tabuchi, M. Ohtake, F. Kirino, and M. Futamoto, J. Magn. Soc. Jpn. **32**, 296–303 (2008).
[26]S. Yuasa, T. Katayama, K. Murata, M. Usukura, and Y. Suzuki, J. Magn. Magn. Mater. **177-181**, 1296 (1998).
[27]C. Bordel, J. Juraszek, D. W. Cooke, C. Baldasseroni, S. Mankovsky, J. Minár, H. Ebert, S. Moyerman, E. E. Fullerton, and F. Hellman, Phys. Rev. Lett. **109**, 117201 (2012).
[28]J. Cao, N. T. Nam, S. Inoue, H. Y. Y. Ko, N. N. Phuoc, and T. Suzuki, J. Appl. Phys. **103**, 07F501 (2008).
[29]G. C. Han, J. J. Qiu, Q. J. Yap, P. Luo, T. Kanbe, T. Shige, D. E. Laughlin, and J.-G. Zhu, J. Appl. Phys. **113**, 123909 (2013).
[30]J. Smit and H. G. Beljers, Philips Res. Rep. **10**, 113 (1955).
[31]A. Butera, J. L. Weston, and J. A. Barnard, J. Magn. Magn. Mater. **284**, 17–25 (2004).
[32]A. Butera, Eur. Phys. J. B **52**, 297–303 (2006).
[33]N. Álvarez, G. Alejandro, J. Gómez, E. Goovaerts, and A. Butera, J. Phys. D: Appl. Phys. **46**, 505001 (2013).
[34]A. Butera, N. Alvarez, G. Jorge, M. M. Ruiz, J. L. Mietta, and R. M. Negri, Phys. Rev. B **86**, 144424 (2012).
[35]A. I. Zakharov, A. M. Kadomtseva, R. Z. Levitin, and E. G. Ponyatovskiĭ, Sov. Phys. JETP **19**, 1348 (1964).
[36]C. Marquina, M. R. Ibarra, P. A. Algarabel, A. Hernando, P. Crespo, P. Agudo, A. R. Yavari, and E. Navarro, J. Appl. Phys. **81**, 2315 (1997).
[37]G. Zheng, S.-H. Ke, M. Miao, J. Kim, R. Ramesh, and N. Kioussis, AIP Adv. **7**, 055914 (2017).